

# Evaluation of Type-IV Creep Damages in Thick Welded Joint for High Cr Steels

M. Tabuchi<sup>1</sup>, H. Hongo<sup>1</sup>, T. Watanabe<sup>1</sup>, K. Sawada<sup>1</sup>, Y. Takahashi<sup>2</sup>

<sup>1</sup> *National Institute for Materials Science, Tsukuba, Japan*

<sup>2</sup> *Central Research Institute of Electric Power Industry, Komae, Japan*

## Abstract

Creep strength of welded joints in high Cr steels decreases due to the formation of Type-IV creep damage in heat-affected zone (HAZ) during long-term use at high temperatures. This paper aims to elucidate the processes and mechanisms of Type-IV failure. Creep rupture and creep interruption tests for the welded joints of Mod.9Cr-1Mo (ASME Gr.91) steel were conducted. Number and area fraction of Type-IV creep voids were measured quantitatively. The measured distributions of creep voids were compared with FEM computations using damage mechanics analysis. It is considered that both the multiaxial stress state and strain concentration in HAZ influence the evolution of creep voids.

## 1. Introduction

High Cr ferritic heat resisting steels have been widely used for boiler components in ultra super critical (USC) thermal power plants operated at about 600°C. Due to their excellent mechanical properties, these steels are also regarded as potential structural materials for the new generation of nuclear power reactors. Fine-grained microstructures with lower creep strength were formed in the HAZ during weld thermal cycle in the ferritic steels. Type-IV creep damages that develop in the fine-grained HAZ under long-term use at high temperatures decrease the creep strength of high Cr steel welds. More than a decade has passed from the practical application of these steels to USC power plants, and Type-IV damages become serious problem for the structural components. Many researches concerning Type-IV damage and failure were conducted from the metallurgical and mechanical aspects [1-3]. However, the mechanisms of Type-IV failure have not been fully understood. In the present paper, creep rupture and creep interruption tests for Mod.9Cr-1Mo steel welds were conducted using large plate type specimens including original plate thickness. Distributions and evolutions of Type-IV creep damages in HAZ of welded joints were measured quantitatively, and were compared with FEM computations using damage mechanics analysis.

## 2. Experimental procedure

The material investigated is a Mod.9Cr-1Mo steel plate 25mm in thickness. The plates were welded by gas tungsten arc welding using double U groove and single U groove. In this paper, we call the welded joint with double U groove as Weld-A, and single U groove as Weld-B, respectively. After welding, post-weld heat treatment was conducted. Creep tests were conducted using the plate type specimen in order to investigate the effect of groove configuration. The S-welded joint specimens shown in Fig. 1(a) were used for creep rupture tests at 550, 600

and 650°C. The L-welded joint specimens 21mm in thickness, 21mm in width and 100mm in gage length, which includes the full original plate thickness, shown in Fig. 1(b) were used for creep interruption tests of Weld-A. Figure 2 shows the cross sectional view of the weld parts of L-welded joint specimen of Weld-A and S-welded joint specimen of Weld-B. After creep, the specimens were cut and creep damages (voids and cracks) in HAZ in the central cross section of specimen width were measured using laser microscope and image analysis software. Measuring method of creep voids is explained in Fig. 3. The distributions of area and number of creep voids along the plate thickness direction were measured. The number density and area fraction of creep voids were calculated as follows:

$$\text{Number density of creep voids} = n / S \quad (1)$$

$$\text{Area fraction of creep voids} = \sum_{i=1}^n S_i / S \quad (2)$$

where,  $n$  is the number of voids,  $S_i$  is the area of void  $i$ , and  $S$  is the measured area.

### 3. Results and discussions

#### 3.1 Processes of Type-IV creep fracture

The creep test results for the base metal and welded joints of the present Mod.9Cr-1Mo steel at 550, 600 and 650°C are shown in Fig. 4. The failure locations of the welded joints are indicated with subscripts attached to the data plots. At all temperatures, the welded joints showed Type-IV failure and their creep strength decreased than base metal for lower stresses and long-term conditions. The differences in creep rupture times between welded joint and base metal tended to widen with increasing temperature and decreasing stress.

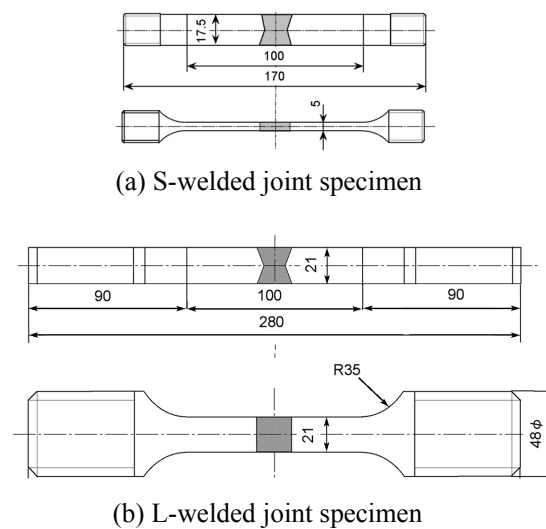


Fig. 1 Creep test specimens of welded joint.

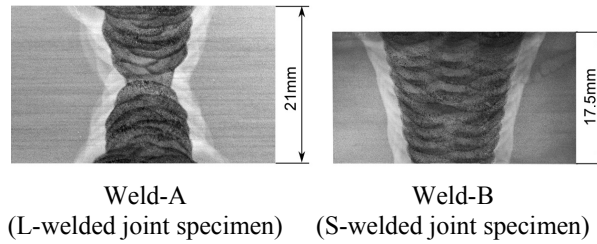


Fig. 2 Cross sectional view of the weld part of the creep test specimens.

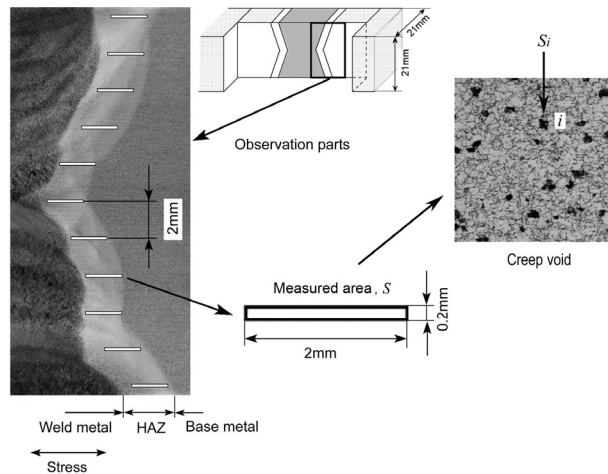


Fig. 3 An example of measuring procedure for creep voids in the HAZ. (Weld-A, L-welded joint specimen)

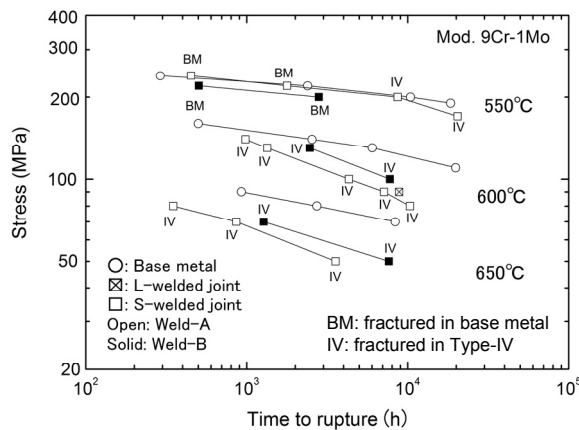


Fig. 4 Creep test results for base metal and welded joint of Mod.9Cr-1Mo steel.

In order to clarify the formation and growth processes of Type-IV damages, creep interruption tests were conducted using the L-welded joint specimen of Weld-A. The creep tests were conducted at 600°C and 90MPa using six specimens, and were interrupted at about 0.1, 0.2, 0.5, 0.7, 0.8 and 0.9 of rupture life 8853h. Figure 5 shows the binary images of creep voids and cracks observed in the HAZ on the central cross section of the L-welded joint specimens after interruption of creep tests. It is found that a small number of creep voids have formed at 2000h

(about 0.2 of life), creep voids increased with elapse of time, and then coalesced to form a crack at 7040h (0.8 of life). The number density and area fraction of creep voids were measured according to the method shown in Fig. 3.

Figure 6 shows distributions of the number density and area fraction of creep voids in HAZ with creep time. This result indicates that creep voids were formed in the area 3-4mm below the surfaces of the plate. The number of creep voids was fewer near the specimen surfaces and the center of thickness. The number density of creep voids increased with elapse of time till 6000h (0.7 of life) and then saturated, while the area fraction of creep voids increased after 6000h. The total number of creep voids per  $1\text{mm}^2$  and average area fraction of creep voids in 11 areas shown in Fig. 3 was plotted against the normalized time by creep rupture time in Fig. 7. Because the creep voids coalesced to form a crack, the number of voids was saturated at about 0.7 of life, whereas the area fraction of voids was

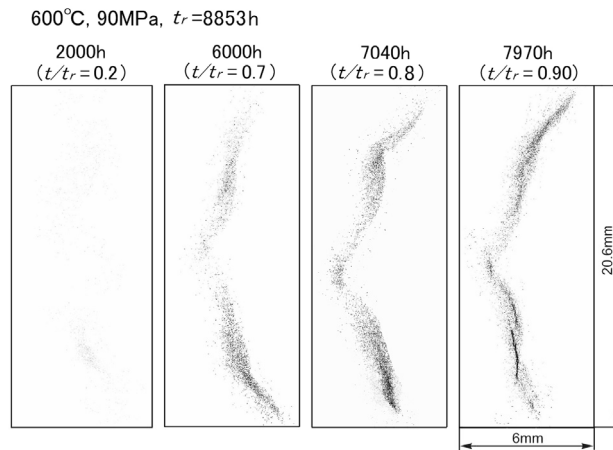


Fig. 5 Binary images of creep damages in HAZ in the central cross section of the L-welded joint after interruption of creep tests.

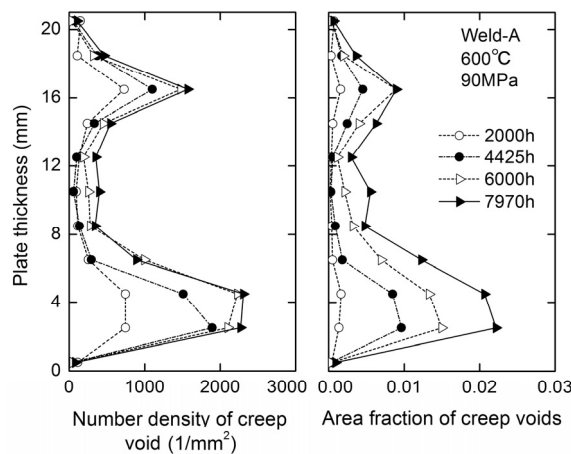


Fig. 6 Measured distributions of the number density and area fraction of creep voids in HAZ of the L-welded joint of Weld-A with time at  $600^{\circ}\text{C}$  for 90MPa.

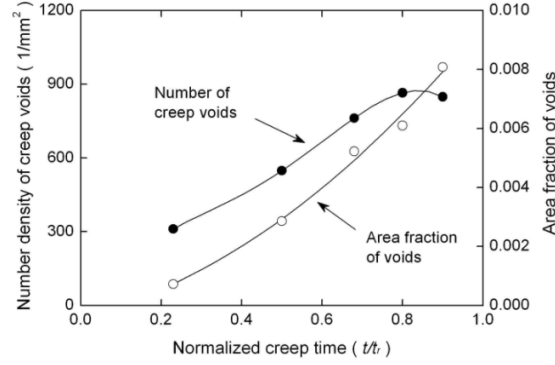


Fig. 7 Evolution of total number of creep voids per 1mm<sup>2</sup> and average area fraction of voids in HAZ of the L-welded joint specimen during creep.

accelerated after that. From these experiments, it was clarified that Type-IV creep voids formed at the early stage of creep life inside the specimen, about 20% below the surface of the plate, increased with elapse of time till 0.7 of life, and then coalesced to form a macro crack at 0.8 of life.

### 3.2 Creep damage analysis

Distributions of stress, strain and creep damage in the L-welded joint specimen of Weld-A were investigated by three-dimensional FEM analysis. The damage mechanics constitutive equation was used for creep analysis as follows [4]:

$$\frac{d\varepsilon_c}{dt} = \frac{3}{2} A \left[ \frac{\sigma_{eq}}{1-\omega} \right]^n \frac{S_{ij}}{\sigma_{eq}} t^m \quad (3)$$

$$\frac{d\omega}{dt} = \frac{M [\alpha\sigma_1 + (1-\alpha)\sigma_{eq}]^\chi}{(1+\phi)(1-\omega)^\phi} t^m \quad (4)$$

where,  $\sigma_1$  is the maximum principal stress,  $\sigma_{eq}$  is the equivalent stress,  $\omega$  is the damage variable, and  $\alpha$  is the parameter that describes materials behavior under triaxial stress state.  $A$ ,  $m$ ,  $n$ ,  $M$ ,  $\phi$  and  $\chi$  are the materials constants. These constants except for  $\alpha$  were decided to best fit the uniaxial creep curves of base metal and simulated fine-grained HAZ (f-HAZ) of the present Mod.9Cr-1Mo steel at 600°C as shown in Table 1. The FE model for the L-welded joint specimen of Weld-A is shown in Fig. 8. The width of the fine-grained HAZ was 1.3mm, which was decided from the microstructural observations. Because the creep test of weld metal was not conducted in this research, materials constants of weld metal were substituted by those of base metal.

Figure 9 shows the distributions of maximum principal stress, equivalent stress, stress triaxial factor ( $TF$ ) and equivalent creep strain in the HAZ on the central cross section of the welded joint with creep at 600°C and 90MPa. The equivalent

creep strain is high near the specimen surfaces and low inside the plate thickness; about 4-16mm from the surface. The  $TF$  increases to about 5.0 with time inside the plate thickness. It shows high values in the areas about 4-16mm from the plate surface, while it is the smallest in the surface areas. In the experimental results of Fig. 6, creep voids are mostly observed at the area 3-4mm below the plate surfaces and are scarcely near the surfaces and center of plate thickness. From the above comparisons, it can be considered that both the concentration of creep strain and the high multiaxial stress condition in fine-grained HAZ influence the distributions of Type-IV creep damages.

Table 1 Materials constants for the Mod.9Cr-1Mo steel at 600°C.

Materials constants	Base metal	Simulated f-HAZ
$A$	1.04E-33	4.07E-23
$N$	13.14	9.16
$M$	-0.530	-0.282
$M$	1.24E-30	1.82E-22
$\phi$	4.5	4.3
$\chi$	12.01	8.99

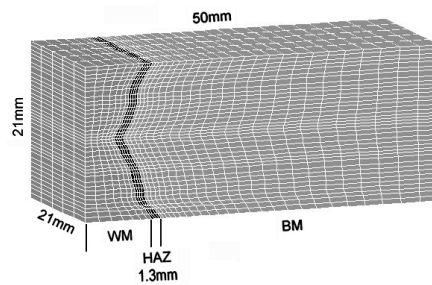


Fig. 8 FE model of L-welded joint specimen of Weld-A.

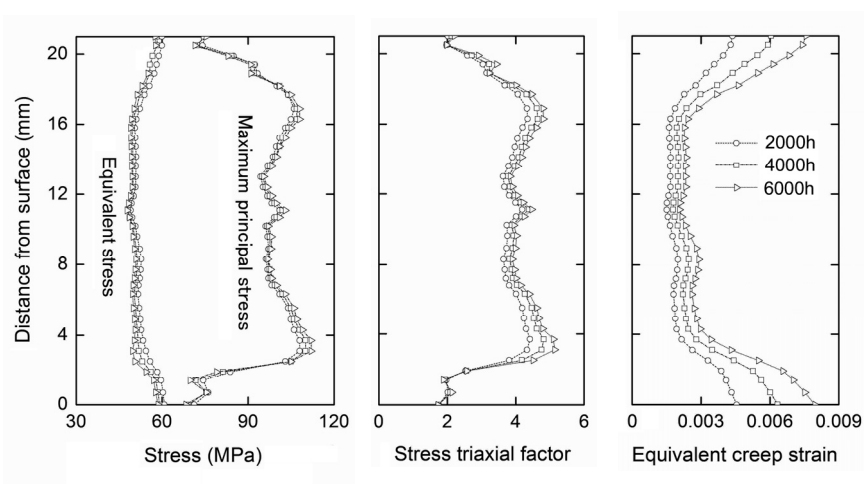


Fig. 9 Distributions of stress,  $TF$  and equivalent creep strain in HAZ in the central cross section of the L-welded joint of Weld-A with creep at 600°C for 90MPa.

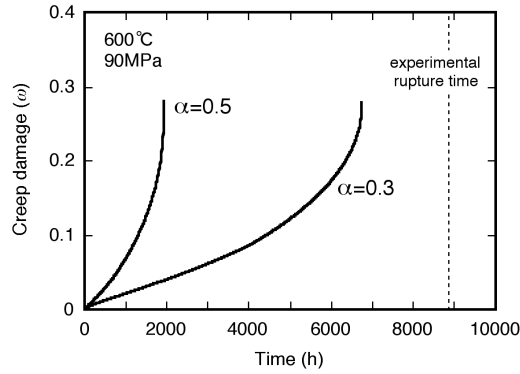


Fig. 10 Changes of creep damage  $\omega$  with time in HAZ of the L-welded joint.

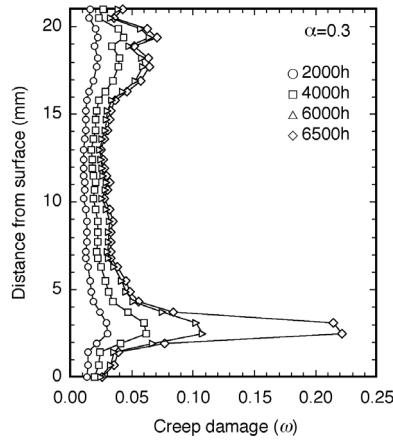


Fig. 11 Distributions of creep damage  $\omega$  in the thickness direction of HAZ for the L-welded joint of Weld-A.

Figure 10 shows changes in the maximum value of creep damage  $\omega$  with time calculated using  $\alpha=0.3$  and  $0.5$ , which compares the predicted life with experimental rupture time for  $90\text{MPa}$  and  $600^\circ\text{C}$ . For the present Mod.9Cr-1Mo steel, it appears that about  $0.3$  is better for  $\alpha$  to predict creep rupture time. Figure 11 shows the calculated distributions of damage  $\omega$  in the HAZ of the central cross section of the L-welded joint for  $\alpha=0.3$ . The creep damage  $\omega$  shows the maximum value in the areas about  $3\text{mm}$  from the specimen surfaces. The computed damage distributions appear to correspond well to the observed distribution of creep voids in Fig. 6. These results mean that it is important to take into account the effect of stress triaxiality, both maximum principal stress and equivalent stress, in life prediction and damage evaluation of high Cr ferritic steel welds.

Creep damage can also be evaluated based on a ductility exhaustion approach. Creep rupture ductility under multiaxial stress condition is given as follows [5]:

$$\frac{\varepsilon_f^*}{\varepsilon_f} = \sinh \left[ \frac{2 \left( \frac{n-1/2}{n+1/2} \right)}{3} \right] / \sinh \left[ 2 \left( \frac{n-1/2}{n+1/2} \right) \frac{\sigma_m}{\sigma_{eq}} \right] \quad (5)$$

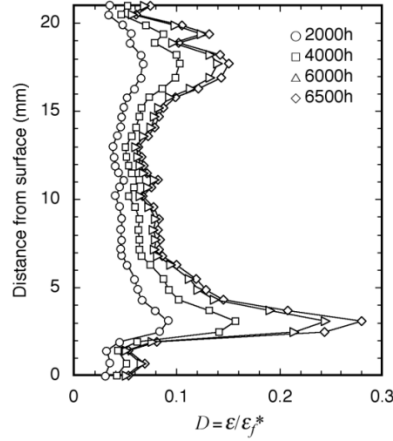


Fig. 12 Distributions of creep damage based on the ductility exhaustion approach in the HAZ along the thickness direction of the L-welded joint specimen.

where,  $\sigma_m$  is the mean stress and  $\epsilon_f^*$  and  $\epsilon_f$  are the rupture strain under multiaxial stress and uniaxial stress condition, respectively. Creep damage can be defined as:

$$D = \epsilon_{eq} / \epsilon_f^* \quad (6)$$

where,  $\epsilon_{eq}$  is the equivalent creep strain. Figure 12 shows the calculated distributions of creep damage in the HAZ using Eq. (6). Creep damages in Fig. 12 peaks at about 3mm below the specimen surfaces: this corresponds closely to the experimental results in Fig. 6. Because the equivalent strain shows a high value in the surface areas and ductility decreases in the central areas of plate thickness due to high stress triaxiality, the creep damage described in Eq. (6) shows a high value in areas about 3mm below the specimen surfaces. It can thus be concluded that both the concentration of creep strain and the high multiaxial stress conditions in HAZ influence the distribution of Type-IV creep damage.

### 3.3 Effect of groove configuration

Figure 13 shows the distributions of number density and area fraction of creep voids along the thickness direction for the S-welded joint of Weld-B at 650°C and 70MPa. For the creep interrupted specimen at 820h (0.6 of life), creep voids were observed in the area from about 3mm below the surfaces to the center of thickness. For the ruptured specimen, a creep crack was observed at the area 3-4mm below the upper surface of the specimen. Creep voids were scarcely observed near the specimen surfaces. Figure 14 shows another case of the Weld-B ruptured for 18331h at 600°C and 80MPa. In this case, creep crack was formed at about 3mm from the lower surface of the specimen, and number and area fraction of creep voids increased around here. For the Weld-B with single U groove, creep voids were formed inside the plate thickness and the crack initiation site was about 3mm from the upper or lower surface of the plate. These results of Figs. 6, 13 and 14 indicate that creep damages were mostly formed in the area about 20% below the surface of the plate for both the Weld-A and Weld-B.

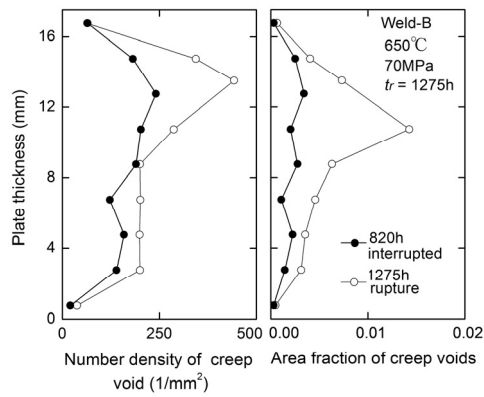


Fig. 13 Creep void distributions of the S-welded joint for Weld-B at 650°C for 70MPa.

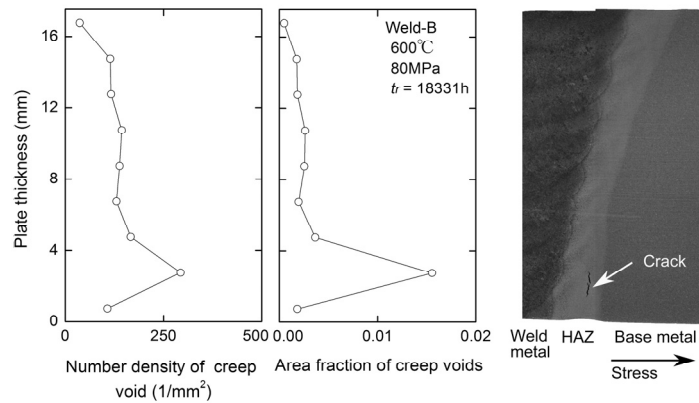


Fig. 14 Creep void distributions of the S-welded joint for Weld-B at 600°C for 80MPa.

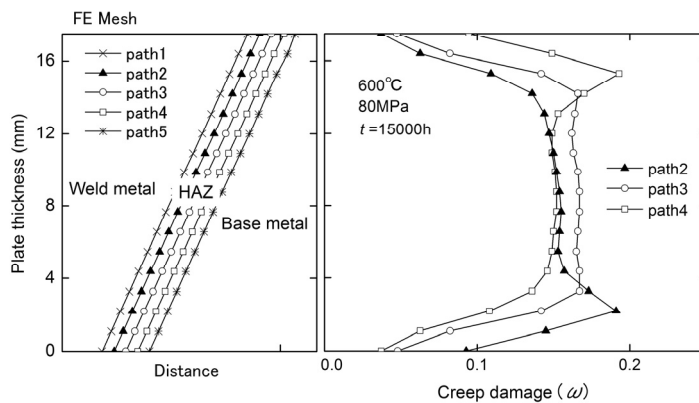


Fig. 15 Distributions of creep damage  $\omega$  in the HAZ along the thickness direction of the S-welded joint specimen of Weld-B (600°C, 80MPa, 15000h).

Figure 15 shows the calculated distributions of damage  $\omega$  in the HAZ of the S-welded joint specimen of Weld-B. Because the distributions of  $\omega$  are dependent on the path in HAZ, the data for each path are plotted in Fig. 15. The creep

damage  $\omega$  shows the higher values inside the plate thickness more than 2-3mm below the surfaces. The maximum value of  $\omega$  locates in the areas 2.2mm below the upper surface for path 4 and 2.2mm below the lower surface for path 2. These computed damage distributions appear to correspond well to the observation results that crack initiation site of Weld-B was about 3mm from the upper or lower surfaces of the plate.

#### 4. Conclusions

Aiming to elucidate the processes and mechanisms of Type-IV failure, distributions and evolutions of creep voids in HAZ of the Mod.9Cr-1Mo steel welds were investigated. Results are summarized as follows;

- (1) Creep voids of Mod.9Cr-1Mo steel weld form at the early stage of creep rupture life (0.2 of life), increase with time till 0.7 of life, and then coalesce to form a macro crack after 0.8 of life. Creep voids mostly form at the area about 20% below the surfaces, inside the plate thickness, for the welded joint with double U groove.
- (2) For the welded joint with single U groove, creep voids increased inside the plate thickness and the creep crack formed at the area about 20% below the upper or lower surface of the plate.
- (3) It can be considered that both the concentration of creep strain and the high multiaxial stress condition in fine-grained HAZ influence the formation of Type-IV creep damages. Stress triaxiality should be taken into account for life prediction and damage evaluation of high Cr ferritic steel welds

#### Acknowledgement

A part of this study was financially supported by the Budget for Nuclear Research of the Ministry of Education, Culture, Sports, Science and Technology, based on screening and counseling by the Atomic Energy Commission.

#### References

- [1] G. Eggeler, A. Ramteke, M. Coleman, B. Chew, G. Peter, A. Burblies, J. Hald, C. Jefferey, J. Rantala, M. deWitte, R. Mohrmann, Analysis of creep in a welded P91 pressure vessel, *Int. J. of Pressure Vessels and Piping* 60 (3) (1994) 237-257.
- [2] J.A. Francis, W. Mazur, H.K.D.H. Bhadeshia, Review: Type-IV cracking in ferritic power plant steels, *Materials Science and Technology* 22 (12) (2006) 1387-1395.
- [3] H. Hasegawa, T. Muraki, M. Ohgami, Identification and formation mechanism of a deformation process determining microstructure of Type-IV creep damage of the advanced high Cr containing ferritic heat resistant steel, *Tetsu-to-Hgane* 92 (10) (2006) 609-617 (in Japanese).
- [4] T.H. Hyde, W. Sun, A.A. Becker, Creep crack growth in welds: a damage mechanics approach to predicting initiation and growth of circumferential cracks, *Int. J. of Pressure Vessels and Piping* 78 (11-12) (2001) 765-771.
- [5] A.C.F. Cocks, M.F. Ashby, Intergranular fracture during power-law creep under multiaxial stress, *Metal Science* 14 (8-9) (1980) 395-402.